First-principles-based $\pm s$-wave modelling for iron-based superconductors: Studies for specific heat and nuclear magnetic relaxation rate

N. Nakai,[1, 2, *] H. Nakamura,[1, 2, 3] Y. Ota,[1, 2] Y. Nagai,[3, 4] N. Hayashi,[1, 5] and M. Machida[1, 2, 3]

[1] CREST(JST), 4-1-8 Honcho, Kawaguchi, Saitama 332-0012, Japan
[2] CCSE, Japan Atomic Energy Agency, 6-9-3 Higashi-Ueno, Taito-ku, Tokyo 110-0015, Japan
[3] TRIP(JST), 5 Sanban-cho, Chiyoda-ku, Tokyo 110-0075, Japan
[4] Department of Physics, University of Tokyo, Tokyo 113-0033, Japan
[5] N2RC, Osaka Prefecture University, 1-2 Gakuen-cho, Naka-ku, Sakai 599-8570, Japan
(Dated: September 7, 2009)

In order to consistently explain controversial experimental results on superconducting states observed by different probes in typical iron-based superconductors, we construct a realistic multi-band $\pm s$-wave pairing model by combining the quasiclassical formalism with the first-principles calculation. The model successfully resolves the controversies in contrast to the fact that simplified models such as two-band $\pm s$-wave one fail to do. A key in the model is the existence of relatively small gaps which leads to material-dependent peculiarities.

The discovery of the iron-pnictide superconductor LaFeAs(O$_{1-x}$F$_x$) [1] made a striking impact on materials science, because this compound includes the element of the most familiar ferromagnetic metal, Fe, as a main component. The transition temperature T_c in the so-called "1111" compounds RFeAs(O$_{1-x}$F$_x$) (R=Pr, Nd, Sm) exceeds 50K, which is the highest except for high T_c cuprates. In addition to the high transition temperature, the variety of related materials is quite rich. For example, "122" compounds $(A_{1-x}B_x)$Fe$_2$As$_2$ (A=Ba, Sr, Ca, B=K, Cs, Na) and "11" compounds Fe(Se$_x$Te$_{1-x}$) are the typical family materials, whose element substitutions are widely possible [2, 3]. In particular, the superconductivity is surprisingly robust against substitutions of Ni and Co for Fe.

In contrast to the discovery rush of family compounds, their superconducting states still remain elusive. There is no established pairing-symmetry model explaining all experimental results consistently. In the early days, puzzling experimental data were reported. In spite of sharp resistivity drops and clear Meissner signals at the superconducting transition T_c, the jump of C/T, where C is the specific heat and T is the temperature, was hardly observable in 1111 compounds. The reason was initially ascribed to a large phonon contribution which masks an electronic one. Afterwards, a small jump at T_c and the concave-down temperature dependence of C/T below T_c were confirmed in not only 1111 compounds [4, 5] but also structurally equivalent LaFeP(O$_{1-x}$F$_x$) [6]. This fact strongly suggests the existence of rather small superconducting gap [7] in addition to large main gaps in the cases of s-wave gap. In this paper, we clarify that such a multi-gap structure consistently explains all experimental observations of 1111 compounds by means of a realistic five-band $\pm s$-wave pairing model based on a first-principles calculation. A striking result of the model is a natural reproduction of the nuclear magnetic relaxation rate $1/T_1$ below T_c.

On the other hand, 122 compounds experimentally exhibit large jumps and exponential behavior in C/T like conventional superconductors [5, 8, 9, 10]. Moreover, the power law in the T-dependence of $1/T_1$ below T_c is different from that of 1111 compounds [3, 11, 12, 13]. In fact, an angle resolved photoemission spectroscopy (ARPES) study reported that all gaps fully open and the difference between their gap amplitudes is not so significant [14]. In this case, we reveal that the multi-gap structure according to ARPES data can consistently explain the specific heat and $1/T_1$ data without any assumptions except for $\pm s$-wave paring symmetry [15, 16]. From the present analyses on 1111 and 122 compounds, it is found that the existence of the relatively small gap gives rise to the material variety. We believe that this fact has an key role on the quest for the superconducting mechanism.

Let us present a procedure to construct the realistic multi-band model. For the band structure around the Fermi level E_F, we perform a first-principles calculation [17], which provides multiple Fermi-surfaces and their density of states (DOS) at E_F depending on the target materials. When evaluating superconducting gaps for multi-band superconductors, we examine all the experimental data and select key data. ARPES measurements are successful for 122 compounds [14]. Therefore, we can directly fit ARPES data to determine the gap amplitudes on each band in the 122 case. On the other hand, ARPES [18] measurements are technically difficult for 1111 compounds. Instead, to estimate the gap amplitudes we adopt data of C/T [6] and the penetration depth [19, 20] in the 1111 case. In fact, those data clearly suggest that the pairing symmetry is full-gap but a small single or small multi gaps coexist with main large gaps [19, 20, 21, 22, 23, 24].

We describe the expression for C/T here, while we refer readers to Refs. [25, 26, 27] for $1/T_1$. The T-dependence
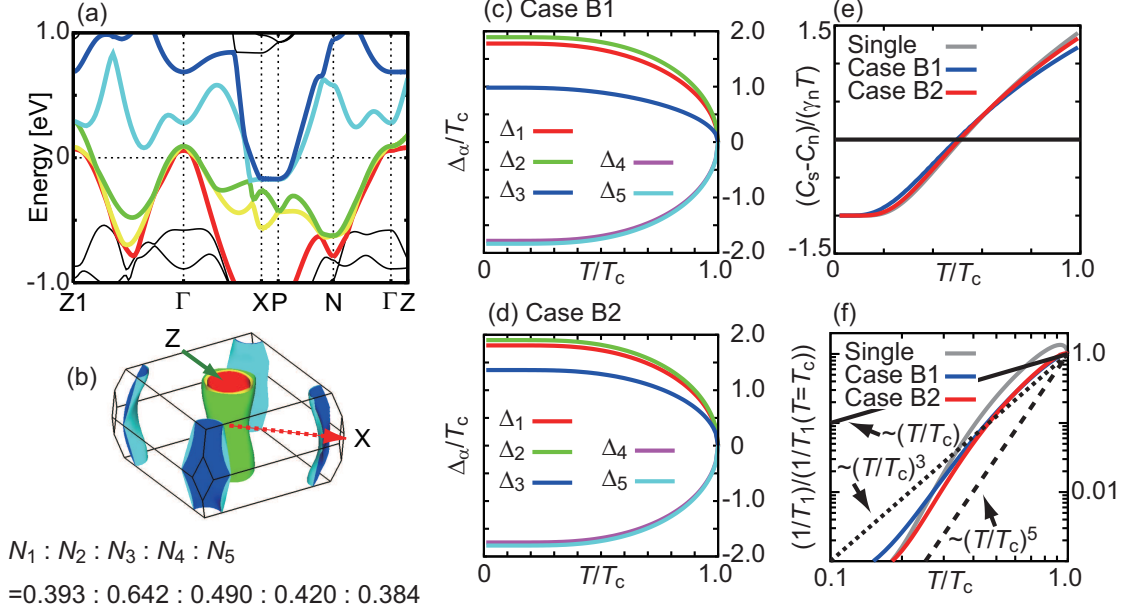
FIG. 1: (color online) (a) The band structure calculated by the generalized gradient approximation using structural measurement values of $BaFe_2As_2$. (b) The Fermi surfaces and the density of states at the Fermi energy. Indices (α=1, 2, 3, 4, 5) are assigned from Γ(zone center) to X. Temperature dependences of the superconducting pair-potential Δ_α are displayed in (c) and (d). Here, "B" of Case B1 or B2 stands for $BaFe_2As_2$. (e) Temperature dependences of $(C_s - C_n)/T$. $C_{s(n)}$ is the specific heat of the superconducting state (normal state). (f) Temperature dependences of the nuclear magnetic relaxation rate $1/T_1$.

of C/T is calculated by the second derivative of the free energy. The free energy can be evaluated by the quasiclassical theory of superconductivity [28, 29], which is a mean field treatment convenient in evaluating superconducting properties. To calculate C/T and $1/T_1$, we need the T-dependence of the multiple superconducting pair-potential Δ_α on each band. For this purpose, we solve the gap equations for multi-band superconductors [30]. With Matsubara frequency $\omega_n = (2n+1)\pi T$, the gap equations are written as

$$\Delta_\alpha = 2\pi T \sum_{\omega_n>0} \sum_\beta \lambda_{\alpha\beta} f_\beta(i\omega_n), \qquad (1)$$

$$\Delta_\alpha^* = 2\pi T \sum_{\omega_n>0} \sum_\beta \lambda_{\alpha\beta} f_\beta^\dagger(i\omega_n). \qquad (2)$$

where α and β stand for the band index, and $\lambda_{\alpha\beta}$ is the effective coupling constant. In addition, $\lambda_{\alpha\beta} = N_\beta \lambda_{\beta\alpha}/N_\alpha$ with N_α being DOS at E_F for α-band. $\lambda_{\alpha\alpha}$ comes from the intra-band interaction, and $\lambda_{\alpha\beta}$, where $\alpha \neq \beta$, gives the pair-hopping between the different bands. The effective coupling constants $\lambda_{\alpha\beta}$'s are employed as parameters to reproduce the experimental results for the superconducting gaps. Again, we note the selected experiment type depending on a kind of the compounds, i.e., ARPES [14] for the 122 compounds, and the specific heat [6] and the penetration depth [19, 20] for the 1111 compounds.

The quasiclassical Green's functions $g_\alpha(i\omega_n)$, $f_\alpha(i\omega_n)$,

and $f_\alpha^\dagger(i\omega_n)$ follow the Eilenberger equations as,

$$\omega_n f_\alpha(i\omega_n) = \Delta_\alpha g_\alpha(i\omega_n), \qquad (3)$$
$$\omega_n f_\alpha^\dagger(i\omega_n) = \Delta_\alpha^* g_\alpha(i\omega_n), \qquad (4)$$
$$g_\alpha^2(i\omega_n) = 1 - f_\alpha(i\omega_n) f_\alpha^\dagger(i\omega_n), \qquad (5)$$

where Re $g_\alpha(i\omega_n) > 0$ for $\omega_n > 0$. The free energy difference between the superconducting and normal states [28, 29, 31, 32], $F_{sn} = F_{super} - F_{normal}$, is expressed as

$$F_{sn} = -2\pi T \sum_\alpha \sum_{\omega_n>0} N_\alpha \left[\frac{1 - g_\alpha(i\omega_n)}{1 + g_\alpha(i\omega_n)} \Delta_\alpha^* f_\alpha(i\omega_n) \right], \qquad (6)$$

which demands the solutions of Eqs. (3), (4), and (5),

$$f_\alpha(i\omega_n) = \frac{\Delta_\alpha}{\sqrt{\omega_n^2 + |\Delta_\alpha|^2}}, \qquad (7)$$

$$f_\alpha^\dagger(i\omega_n) = \frac{\Delta_\alpha^*}{\sqrt{\omega_n^2 + |\Delta_\alpha|^2}}, \qquad (8)$$

$$g_\alpha(i\omega_n) = \frac{\omega_n}{\sqrt{\omega_n^2 + |\Delta_\alpha|^2}}. \qquad (9)$$

Note that $f_\alpha^{(\dagger)}(i\omega_n) \to 0$ and $g_\alpha(i\omega_n) \to 1$ when $\omega_n \gg |\Delta_\alpha|$. The cut-off frequency ω_c is introduced as $\sum_{\omega_n>0}^{\omega_c}$ in Eqs. (1), (2) and (6) [33]. Equation (6) indicates that F_{sn} can be directly evaluated by DOS N_α obtained from first-principle calculations and the gap values Δ_α.
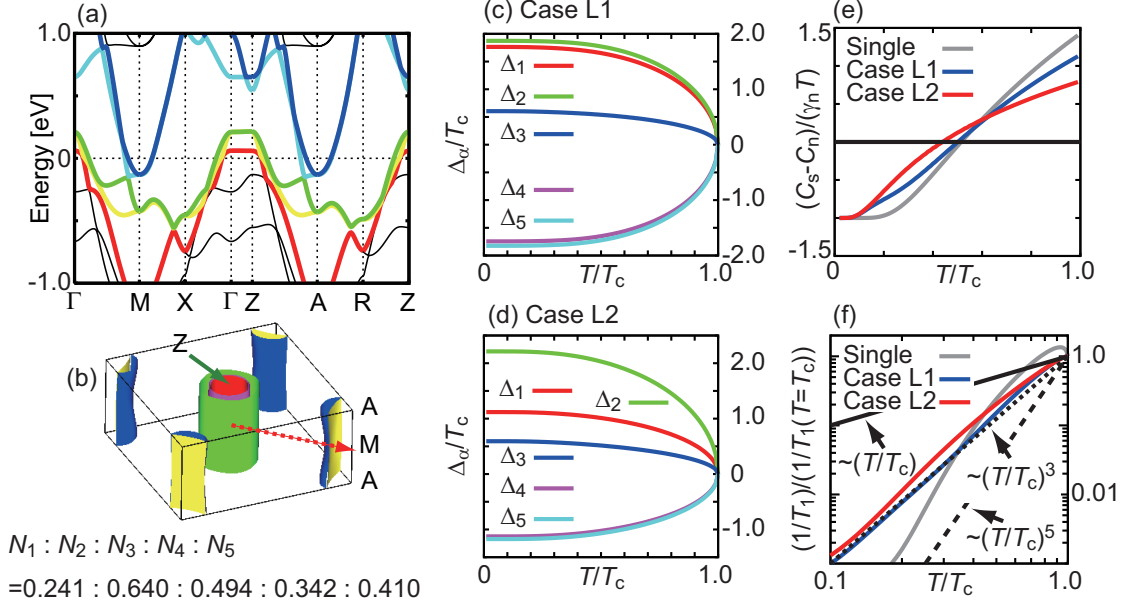
FIG. 2: (color online) (a) The band structure calculated by the generalized gradient approximation using structural measurement values of LaFeAsO. (b) The Fermi surfaces and the density of states at the Fermi energy. Indices (α=1, 2, 3, 4, 5) are assigned from Γ(zone center) to M. Temperature dependence of the superconducting pair-potential Δ_α in (c) and (d). Here, "L" of Case L1 or L2 stands for LaFeAsO. (e) Temperature dependences of $(C_s - C_n)/T$. $C_{s(n)}$ is the specific heat of the superconducting state (normal state). (f) Temperature dependences of the nuclear magnetic relaxation rate $1/T_1$.

Since C/T at constant volume is generally obtained by $C/T = \partial S/\partial T = -\partial^2 F/\partial T^2$, the specific heat in the superconducting state is expressed as

$$\frac{C_s - C_n}{T} = -\frac{\partial^2 F_{sn}}{\partial T^2}, \qquad (10)$$

where $C_{s(n)}$ is the specific heat of the superconducting state (normal state). We can rewrite C_n/T as γ_n, which is the Sommerfeld coefficient. Thus, we numerically calculate $\partial^2 F_{sn}/\partial T^2$ to obtain C_s/T. As for $1/T_1$ [25, 26, 27], we calculate it using N_α and Δ_α obtained here.

Let us present the calculated results. The first focus is 122 compounds. Figure 1(a) shows the band structure of $BaFe_2As_2$. This result is obtained by using the generalized gradient approximation (GGA) based on the measured structural data [2]. The obtained Fermi surfaces are displayed in Fig. 1(b). The calculation gives DOS's at E_F, which are input parameters in the gap equations (1) and (2) and the free energy (6). Each DOS at E_F is written as N_α, where α is numbered as $\alpha = 1, 2, 3, 4, 5$ from Γ point (zone center) to X as shown in Fig. 1(b), and $\alpha = 1$ to 3 (4 to 5) correspond to hole (electron) bands. Throughout this paper, we adopt $\pm s$-wave pairing model since other choices fail to reproduce the experimental data consistently. The positive (negative) sign is assigned to Δ_α of hole (electron) bands (Δ_α are assumed to be real). The T-dependence of Δ_α is calculated so as to follow the ARPES result [14] (Case B1) as shown in Fig. 1(c). On the other hand, in Fig. 1(d)

we show, for comparison, the result (Case B2) with the minimum $|\Delta_3|$ being slightly bigger than the ARPES result. Figure 1(e) shows the T-dependences of C/T. Both Cases B1 and B2 show no significant difference from the weak coupling single-band Bardeen-Cooper-Schrieffer (BCS) result. One of the reasons is that the weighting of the small-gap band is small compared to total one, i.e., the ratio N_3/N_t is 0.2, where N_t is the total DOS ($N_t = \sum_\alpha N_\alpha$). Moreover, the gap-amplitude difference between the minimum $|\Delta_3|$ and the maximum $|\Delta_2|$ is not so large, where $|\Delta_3|/|\Delta_2| \sim 0.5$ (~ 0.7) for Case B1 (B2). On the other hand, the influence of $|\Delta_2|/T_c \sim 2$, which is bigger than the single-band's value 1.76, slightly enhances C/T at T_c. As a result, the difference in C/T becomes small among Case B1, B2 and single-band case. The T-dependences of C/T in Cases B1 and B2 are consistent with the experimental observations [5].

On T-dependence of $1/T_1$, both the cases show significant differences from the single-band BCS case as shown in Fig. 1(f). The coherence peak just below T_c is absent in both Cases B1 and B2, because the cancellation between "+" and "−" signs of Δ_α is effective. In contrast, in the single-band BCS case, even if the damping rate of the quasiparticle is taken large as $\eta = 0.1T_c$, the peak is clearly identified as seen in Fig. 1(f). Moreover, the low-lying excitation arising from the small gap $|\Delta_3|$ alters T-dependence of $1/T_1$ compared to the single-band s-wave case. We point out that the five-band model Case B1

successfully reproduces the experimental results of C/T and $1/T_1$ [5, 13].

We next turn to 1111 compounds. At first, based on GGA with measured structural parameters [34], we obtain the band structure of LaFeAsO as shown in Fig. 2(a). The band index is also numbered as $\alpha = 1, 2, 3, 4, 5$ from Γ (zone center) to M. The five Fermi surfaces are displayed in Fig. 2(b), where N_1, N_2, N_3 (N_4, N_5) are the DOS at $E_{\rm F}$ of hole (electron) bands. We prepare two types of multi-gap structures, Cases L1 and L2, whose T-dependences of Δ_α are plotted in Figs. 2(c) and 2(d), respectively. These are estimated by experimental data of C/T [4, 5, 6] and the penetration depth [20], because direct experimental ARPES data of the gaps are not presently available in 1111 compounds. Case L1 gives four large gaps and one small gap, while Case L2 considers a medium gap between the maximum and minimum gap-amplitudes. Figure 2(e) shows T-dependence of C/T for both Cases L1 and L2. When the amplitude difference between the minimum and maximum gaps is large, the jump of C/T at $T_{\rm c}$ decreases. For comparison, we note that the small gap in the 122 compounds as shown in Fig. 1(e) is not enough to reduce the jump of C/T like the present 1111 compound case. In addition, Case L2 reproduces the concave-down behavior as observed in LaFeP(O$_{1-x}$F$_x$) [6]. Thus, the small-jump feature and the concave-down behavior in C/T suggest not only the existence of a small-gap but also that of a medium-gap band, whose contributions are significant compared to 122 compounds. We then expect that Case L2 is the most possible candidate.

Figure 2(f) shows T-dependence of $1/T_1$ for both Cases L1 and L2. We find that both Cases L1 and L2 surprisingly exhibit T^3-behavior of $1/T_1$ up to the experimentally accessible low T. The low-lying excitations due to the small gap push the exponential behavior of $1/T_1$ into a further lower temperature region. Moreover, the peak just below $T_{\rm c}$ does not appear because of the cancellation due to $\pm$ signs [27]. The most of 1111 compounds show T^3 dependence in $1/T_1$ below $T_{\rm c}$ [3, 13], which suggests that Case L2 is the best as noted in Fig. 2(f).

In conclusion, we examined the validity of $\pm s$-wave scenario for typical iron-based superconductors (122 and 1111 compounds) through the realistic model using the quasiclassical formalism combined with first-principles calculations. Consequently, we found that any anomalous properties observed in the specific heat and the nuclear magnetic relaxation rate are reproducible without any extrinsic assumptions, i.e., all required is the properly-evaluated gap amplitude of each band.

Finally, we add a note that the momentum dependence of the gap amplitudes is reported by some recent experiments [35, 36, 37] of the related compound. Such an anisotropy can be easily implemented in the present framework.

* nakai.noriyuki@jaea.go.jp
[1] Y. Kamihara *et al.*, J. Am. Chem. Soc. **130**, 3296 (2008).
[2] M. Rotter *et al.*, Phys. Rev. B **78**, 020503(R) (2008).
[3] K. Ishida *et al.*, J. Phys. Soc. Jpn. **78**, 062001 (2009).
[4] L. Ding *et al.*, Phys. Rev. B **77**, 180510 (2008).
[5] G. Mu *et al.*, Phys. Rev. B **79**, 174501 (2009).
[6] Y. Kohama *et al.*, J. Phys. Soc. Jpn. **77**, 094715 (2009).
[7] D. V. Evtushinsky *et al.*, New J. Phys. **11**, 055069 (2009).
[8] S. L. Bud'ko *et al.*, Phys. Rev. B **79**, 220516(R) (2009).
[9] N. Kurita *et al.*, Phys. Rev. Lett. **102**, 147004 (2009).
[10] F. Ronning *et al.*, Phys. Rev. B **79**, 134507 (2009).
[11] H. Fukazawa *et al.*, J. Phys. Soc. Jpn. **78**, 033704 (2009).
[12] Y. Kobayashi *et al.*, J. Phys. Soc. Jpn. **78**, 073704 (2009).
[13] M. Yashima *et al.*, arXiv:0905.1896.
[14] K. Nakayama *et al.*, Euro Phys. Lett. **85**, 67002 (2009).
[15] I. I. Mazin *et al.*, Phys. Rev. Lett. **101**, 057003 (2008).
[16] K. Kuroki *et al.*, Phys. Rev. B **79**, 224511 (2009).
[17] The density functional calculation package employed throughout this paper is VASP. G. Kresse and J. Hafner, Phys. Rev. B **47**, 558 (1993); G. Kresse and J. Furthmüller, Phys. Rev. B **54**, 11169 (1996).
[18] T. Kondo *et al.*, Phys. Rev. Lett. **101**, 147003 (2008).
[19] K. Hashimoto *et al.*, Phys. Rev. Lett. **102**, 017002 (2009).
[20] C. Martin *et al.*, Phys. Rev. Lett. **102**, 247002 (2009).
[21] C. Martin *et al.*, Phys. Rev. B **80**, 020501(R) (2009).
[22] L. Ding *et al.*, arXiv:0906.0138.
[23] X. G. Luo *et al.*, arXiv:0904.4049.
[24] M. A. Tanatar *et al.*, arXiv:0907.1276.
[25] B. Mitrovic and K. V. Samokhin, Phys. Rev. B **74**, 144510 (2006).
[26] Y. Bang *et al.*, Phys. Rev. B **79**, 054529 (2009).
[27] Y. Nagai *et al.*, New J. Phys. **10**, 103026 (2008).
[28] G. Eilenberger, Z. Phys. **214**, 195 (1968).
[29] N. Kopnin, *Theory of Nonequilibrium Superconductivity* (Oxford University Press, New York, 2005), Chap. 5.
[30] H. Suhl *et al.*, Phys. Rev. Lett. **3**, 552 (1959).
[31] K. Watanabe and T. Kita, J. Phys. Soc. Jpn. **73**, 2239 (2004).
[32] V. G. Kogan *et al.*, Phys. Rev. B **80**, 014507 (2009).
[33] $\omega_{\rm c} = 2000T_{\rm c}$ is used in calculating pair potentials and free energy. To obtain the second derivative of F_{sn} precisely by numerical derivative, we need such a large $\omega_{\rm c}$.
[34] C. de la Cruz *et al.*, Nature **453**, 899 (2008).
[35] M. Yamashita *et al.*, arXiv:0906.0622.
[36] H. Fukazawa *et al.*, J. Phys. Soc. Jpn. **78**, 083712 (2009).
[37] K. Hashimoto *et al.*, arXiv:0907.4399.